Journal of Applied Fluid Mechanics, Vol. 13, No. 6, pp. 1719-1726, 2020.
Available online at www.jafmonline.net, ISSN 1735-3572, EISSN 1735-3645.
DOI: 10.47176/jafm.13.06.31492

Effect of Circumferential Casing Treatment on Low-Speed Contra-Rotating Fans

M. Heinrich[1†], H. Khaleghi[2] and C. Friebe[3]

[1] *Institute of Mechanics and Fluid Dynamics, Technical University Bergakademie Freiberg, Lampadiusstraße 4, 09599 Freiberg, Germany*
[2] *Department of Aerospace Engineering, Amirkabir University of Technology, No 350, Hafez Ave, Valiasr Square, Tehran, Iran*
[3] *Institute of Air Handling and Refrigeration (ILK), Bertolt-Brecht-Allee 20, 01309 Dresden, Germany*

†*Corresponding Author Email: Martin.Heinrich@imfd.tu-freiberg.de*

(Received February 17, 2020; accepted May 5, 2020)

ABSTRACT

The benefits of circumferential groove casing treatment on the performance of a low-speed contra-rotating fan are investigated. Three-dimensional, time-dependent simulations are carried out with the *k-ω* SST-SAS hybrid turbulence model using the open-source CFD library OpenFOAM. The numerical model is validated with experimental data from the contra-rotating fan with a smooth casing. This comparison showed a very good agreement. Then, two casing treatment variations are analyzed: 1) circumferential grooves on top of the front rotor, and 2) circumferential grooves on top of the rear rotor. Simulating the performance curve at design speed reveals an increase in pressure rise for casing treatment at the front rotor of up to 4 %. This results from significantly reduced blade pressure fluctuations and weakened blade tip vortices at the front rotor. A weaker tip leakage vortex leads to a less disturbed inflow for the rear rotor and thus pressure fluctuations. In contrast, grooves on top of the rear rotor offer no positive effect since there is no rotor downstream to benefit from reduced fluctuations or weakened tip leakage vortex. Pressure probes downstream of the rear rotor were evaluated using FFT. Grooves reduce the magnitude of blade passing frequencies and their harmonics while partly increasing lower frequencies.

Keywords: Contra-rotating fan; Circumferential groove casing treatment; CFD; Blade tip vortex.

NOMENCLATURE

C	constant in turbulence model
k	turbulent kinetic energy
L_T, L_{vK}	length scales in turbulence model
p	pressure
Q	flow rate
Q_{SAS}	additional term in SAS turbulence model
S_{ij}	deformation tensor
t	time
T_1, T_2	variables in turbulence model
$\boldsymbol{u}$	velocity vector
y^+	dimensionless wall distance
κ	constant in turbulence model
ν	fluid viscosity
ξ_2	constant in turbulence model
ρ	fluid density
σ_ϕ	constant in turbulence model
τ	viscous shear tensor
τ^{RS}	Reynolds stress tensor
ω	specific dissipation

1. INTRODUCTION

Contra-rotating fans or compressors are one approach to increase performance and extend the range of application of turbomachines compared to conventional single-rotor machines with guide vanes. A rear rotor is used to add more energy to the fluid and recover kinetic energy from the outlet swirl of the first rotor, which would otherwise be lost. Compact design and therefore reduced weight and size make their use beneficial for various applications, such as high-speed propulsion systems, or tunnel and mine ventilation.

A lot of research work was published in recent years regarding contra-rotating fans and the influence of various design parameters. Wang *et al.* (2013)

compared a contra-rotating fan with a single-rotating fan with guide vanes. Their results revealed an increased pressure coefficient and efficiency at lower rotational speed and given power consumption. The effect of rotor-rotor distance has been investigated by various researchers, e.g. Nouri *et al.* (2012) and Sharma *et al.* (1988). The combination of rotational speeds of the front and rear rotor played a significant role in the stage performance. Mistry and Pradeep (2012) found out that a higher speed of the rear rotor resulted in an increased pressure rise. Furthermore, this also led to a significant improvement in stall-free range and better off-design performance as shown by Nagano *et al.* (1971), Sharma *et al.* (1985), and Chen *et al.* (2008). Roy *et al.* (1992) summarized from their results that the front rotor mainly affects the flow capacity whereas the rear rotor affects the pressure rise and operating range.

Tip clearance size effects on the performance and tip leakage vortex of a contra-rotating fan were investigated by Wang *et al.* (2014). Stable operating range and isentropic efficiency were reduced with increasing tip clearance size. Negative effects due to tip clearance were much more prominent on the rear rotor which ultimately led to compressor breakdown. Aerodynamic instabilities, such as rotating stall and surge, limit the operating range of a fan or compressor. Therefore, employing passive and active stall control methods postpone stall inception and enhance operability. These methods include casing treatment, endwall injection, and recirculation. Most research is focused on circumferential casing treatment on axial compressors, e.g. Bailey (1972), Muller *et al.* (2007), Rabe *et al.* (2002), and Wu *et al.* (2010). However, the number of investigations regarding stall control methods in contra-rotating low-speed fans is very limited.

In particular, there are only two publications about the application of casing treatment in contra-rotating fans and compressors. Pundhir *et al.* (1990) experimentally investigated different casing treatment configurations on a low-speed contra-rotating axial compressor. Their work included solid casing, axial slots, skewed slots, and circumferential grooves. They concluded that circumferential grooves increased stall margin and stage pressure rise coefficient by up to 14.5% and 8%, respectively. At the same time, the axial slot type casing impaired stage pressure rise. A second investigation regarding casing treatment was conducted by Mao *et al.* (2018). They numerically analyzed the impact of circumferential grooves on top of the second rotor in a counter-rotating axial-flow compressor. Compressor performance improved near stall conditions, while there was almost no influence near peak efficiency point. Furthermore, the stall margin rose and the intensity of pressure fluctuations decreased. However, these improvements were much weaker compared to the findings by Pundhir *et al.* (1990).

Although only two publications investigated circumferential grooves for contra-rotating low-speed axial fans, they clearly show the benefits of this type of casing treatment. However, it seems unclear how the placement of grooves on either the front or rear rotor affects the stage performance and the unsteady flow field. Therefore, this work focuses on the placement of circumferential grooves and investigates their applicability for low-speed contra-rotating axial fans.

2. EXPERIMENTAL SETUP

The contra-rotating fan for this investigation was designed using CFturbo (2017). This software relies on 1D-balance equations, empirical correlations, and airfoil theory. The conditions for each rotor are based on the power distribution (120 Pa and 60 Pa) and the corresponding rotational speeds. Each stage has a straight leading and trailing edge with 7 blades at the front and 5 blades at the rear rotor. The complete fan is designed for a volumetric flow rate of Q = 0.486 m^3/s and a total pressure rise of Δp = 180 Pa. Table 1 summarizes its design parameters.

Table 1 Summary of fan parameters

Parameter	Unit	Front rotor	Rear rotor
Hub diameter	mm	195	
Fan diameter	mm	307	
Tip clearance	mm	3	
Solidity	-	0.25	
No. of blades	-	7	5
Design speed	1/s	32	20
Pressure rise	Pa	120	60
Flow rate	m^3/s	0.486	

Kerscher *et al.* (2017) and Krause *et al.* (2018) carried out the experimental measurements with a pipe at the suction side and an open outlet at the pressure side of the fan (see Fig. 1). The operating point is set by adjusting the pressure drop through a throttle valve. The flow rate is measured at the inlet nozzle using four pressure tabs (Ashcroft XLDP2 TSI VELOCICALC Model 9565) at the tube walls. Four wall pressure tabs are also used at the suction side of the fan to measure the pressure rise against the environment. The rotational speed for both fans is measured using a laser tachometer (Compac Visible Optical Sensor).

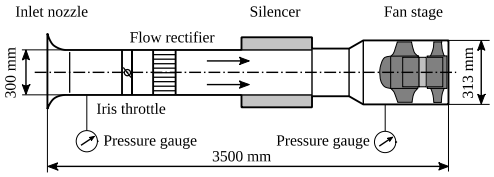

Fig. 1 Testrig for performance measurements.

The accuracy of the measurements at design point is as follows:

- Flow rate: (0.468 ± 0.005) m^3/s
- Pressure rise: (180 ± 0.9) Pa
- Rotational speed (32 ± 0.017) s^{-1}

3. NUMERICAL SETUP

OpenFOAM (2018), an open-source CFD library, is used to solve the governing equations for the contra-rotating fan. The three-dimensional, incompressible, transient, and Reynolds-averaged Navier-Stokes equations are as following:

$$\nabla \cdot \boldsymbol{u} = 0\,, \tag{1}$$

$$\frac{\partial \boldsymbol{u}}{\partial t} + \nabla \cdot (\boldsymbol{u}\boldsymbol{u}) = -\nabla\left(\frac{p}{\rho}\right) + \nabla \cdot \left(\boldsymbol{\tau} + \boldsymbol{\tau}^{\mathrm{RS}}\right) \tag{2}$$

with density ρ, velocity $\boldsymbol{u}$, pressure p, and viscous and Reynolds stress tensor ($\boldsymbol{\tau}$ + $\boldsymbol{\tau}^{\mathrm{RS}}$). Large eddy simulations (LES) for turbomachinery flows are costly and very time consuming due to the necessity of a very fine grid. Therefore, the hybrid approach Scale Adaptive Simulation (SAS) is employed to achieve a compromise between LES and URANS. This hybrid model is based on the Shear Stress Transport (SST) $k-\omega$ turbulence model by Menter (1994) and was proposed by Egorov and Menter (2008). It employs an additional term $\boldsymbol{Q}_{\mathrm{SAS}}$ in the specific dissipation equation:

$$Q_{\mathrm{SAS}} = \max(T_1 - T_2, 0) \tag{3}$$

with

$$T_1 = \xi_2 \kappa \left|S_{ij}\right|^2 \left(\frac{L_T}{L_{vK}}\right)^2, \tag{4}$$

$$T_2 = C\,\frac{2k}{\sigma_\phi} \max\left(\frac{|\nabla\omega|^2}{\omega^2}, \frac{|\nabla k|^2}{k^2}\right), \tag{5}$$

the turbulent length scale L_T, the von Kármán length L_{vK}, and the model constants ξ_2 = 3.51, σ_ϕ = 0.667, κ = 0.41, and C = 2.0. The Q_{SAS} term relieves the turbulence model from turbulent viscosity in strong unsteady regions. In the case of small L_{vK} compared to L_T, the term T_1 dominates and thus Q_{SAS} yields positive values. As a result, ω increases and this eventually leads to a reduction in turbulent viscosity.

Pressure-velocity coupling is performed using the PIMPLE algorithm, a combination of the PISO algorithm by Issa (1986) and the SIMPLE algorithm by Caretto *et al.* (1972). Temporal discretization is second-order backward with a time-step size of 1×10^{-6} s. This results in a maximum Courant number of about 3. The Linear Upwind Stabilized Transport (LUST) scheme is used for spatial discretization of the momentum and second-order limited for the remaining terms. The physical time simulated is 0.2 s, which resolves around six rotations of the first rotor. Using a steady-state solution as an initial condition reduces the computational cost of the transient simulation. After two rotations the flow is assumed to be quasi-steady state. Therefore, the flow field is averaged over the remaining four rotations for postprocessing. The total computing time for each operating point is around 10 days on 168 CPUs.

The numerical model consists of a stationary inlet pipe, the front stage, the rear stage, and the stationary outlet pipe (see Fig. 2). A full 360° model for both stages is used with arbitrary mesh interfaces between all four parts. Thus, no circumferential averaging is performed (e.g. no mixing plane) and all time-dependent blade-to-blade interactions are captured. The inlet and outlet pipe are extended to reduce the influence of the corresponding boundary conditions. The mounting between both rotors is neglected to simplify the numerical model. The stationary and rotating walls are defined as no-slip and adiabatic. A mapped boundary condition is used at the inlet to create a fully developed turbulent flow profile. This way no specific values for k and ω have to be supplied since those will result from the mapping process. The average velocity at the inlet is varied to simulate different operating points. Relative static pressure p/ρ at the inlet is set to zero gradient and to zero value at the outlet with respect to ambient conditions. Other variables at the outlet are treated as zero gradient. The air is defined as a Newtonian fluid with a kinematic viscosity of $\nu = 1.568 \times 10^{-5}$ m^2/s and a density of $\rho = 1.225$ kg/m^3.

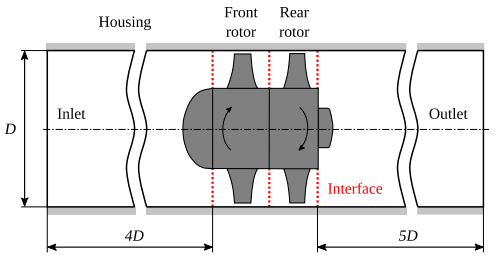

Fig. 2. Numerical model for the CFD simulations.

The inlet and outlet pipes consist of an unstructured, hexahedral mesh with prism layers created by the OpenFOAM meshing tool snappyHexMesh. It is refined towards the housing and the hub of the fan. The structured hexahedral mesh of both fan stages is created with ANSYS TurboGrid (2018). The tip gap of 3 mm size is resolved using 12 × 13 cells in axial and radial direction, respectively. The front and rear rotors consist of 2.7×10^6 and 2.0×10^6 cells, respectively. The mesh is shown in Fig. 3. The total cell count including inlet and outlet is 7.9×10^6 cells. Mesh quality is as follows: maximum skewness of 2.4, non-orthogonality of less than 55°, and an aspect ratio of less than 20. An all-y^+ wall function is employed to model near-wall turbulence. This is required since the average y^+ value is 10 for the blades and less than 5 for the housing and hub. This is a compromise between accuracy and computational cost. Completely resolving the boundary layer up to y^+ = 1 requires a significant number of additional cells and therefore computing time for a fully transient simulation.

Circumferential grooves are used as casing treatment on top of either the front or the rear rotor of the contra-rotating fan. Their position and size are shown in Fig. 4. Four grooves are located on top of the front rotor for the first configuration and six grooves on top of the rear rotor for the second configuration. The rear rotor has more grooves due to the larger chord length. Groove height and width are 3 mm and they are evenly distributed between

leading and trailing edge of the blades. Their design and dimensions are correlated to similar publications of Pundhir *et al.* (1990) and Mao *et al.* (2018). The former work focused on 3 mm × 3 mm grooves at a fan diameter of 486 mm and the latter on 2 mm × 2 mm grooves at a fan diameter of 400 mm. Therefore, the relative size of the grooves investigated in this paper is slightly larger based on the fan diameter. The mesh size of each groove is 12 × 12 × 300 cells in axial, radial, and circumferential directions, respectively. They are meshed separately and connected to the rotors via Arbitrarily Coupled Mesh Interfaces (ACMI).

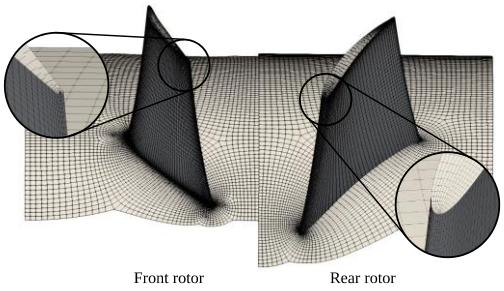

Fig. 3. Computational mesh of one blade passage without inlet and outlet region.

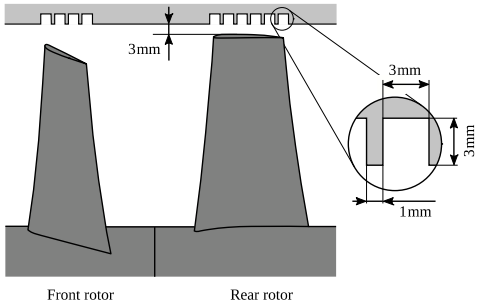

Fig. 4. Circumferential groove position on top of the front and rear rotor.

Total pressure rise of the contra-rotating fan Δp_{tot} is defined as the sum of static pressure between the inlet (index: in) and outlet (index: out) plus the difference in dynamic pressure between fan and inlet:

$$\Delta p_{tot} = (p_{out} - p_{in}) + \frac{\rho}{2}\left(c_{crf}^2 - c_{in}^2\right) \quad (6)$$

with the absolute velocity c in axial direction at the inlet and the fan stage (index: crf). It should be noted that this equation is only valid for incompressible low Mach number flows. Furthermore, probes located downstream of the rear rotor are used to characterize static and total pressure rise and absolute flow angle past the contra-rotating fan.

4. RESULTS

4.1 Validation

At first, the numerical model is validated against the experimental measurements for a smooth casing to assess its accuracy. The CFD simulation offers a very good agreement compared to the experimental results for a smooth casing (see Fig. 5, left). Peak pressure rise is 185 Pa at a flow rate of about 0.42 m^3/s. The decrease in pressure rise at lower flow rates is predicted correctly and the slopes match very well. However, the pressure rise is slightly overpredicted at higher flow rates. This might result from neglecting the mountings located between the front and rear rotors. Including them would lead to higher losses due to friction and therefore to a reduced pressure rise. Although measured in the experiment, operating points in deep stall below 0.275 m^3/s were not simulated. As a conclusion, the numerical model is very well capable of computing the performance of the low-speed contra-rotating fan and will be used to predict the influence of groove casing treatment in the following section.

4.2 Groove Performance

Two different casing treatment configurations are compared in this publication. Configuration A has circumferential grooves on top of the front rotor and configuration B has circumferential grooves on top of the rear rotor. The smooth casing without any modifications is used as a reference.

Figure 5 (right) shows the pressure rise of each configuration for a flow rate of (0.275 - 0.585) m^3/s. At lower flow rates and thus unstable off-design conditions, front grooves yield the best results. The pressure rise is increased by up to 4 % at 0.275 m^3/s and by more than 1 % at 0.425 m^3/s. As a downside, rear grooves lead to a slightly inferior pressure rise at 0.275 m^3/s and otherwise similar performance compared to a smooth casing. At flow rates above 0.425 m^3/s, a smooth casing offers the best results, though. In this stable operating range, grooves do not offer any benefit.

Circumferential grooves increase the cross-sectional area in the tip clearance. Therefore, fluid is accelerated radially, enters the grooves, and is pushed in circumferential direction. Pressure differences between suction and pressure side of the rotor are reduced and thus the blade loading (see Mao *et al.* (2018)). As a result, the pressure-driven tip-leakage flow is weakened as well as the losses associated with it. This positive effect of casing treatment is noticeable only at lower flow rates when blade loading is high and tip-leakage flows are strong. At higher flow rates, the pressure loss due to flow inside the groove cavities reduces the total pressure rise slightly compared to a smooth casing treatment.

Two main effects determine the complex flow field inside the grooves. The first effect is the radial flow velocity at the groove inlet. Between two blades, there is an inflow at the front side and an outflow at the backside of the groove. The second effect is the circumferential velocity of the fluid inside the grooves. It moves in the same circumferential direction as the corresponding blade. This is illustrated in Fig. 6. Both effects are interrupted once a blade passes. At this point, fluid gets pushed into

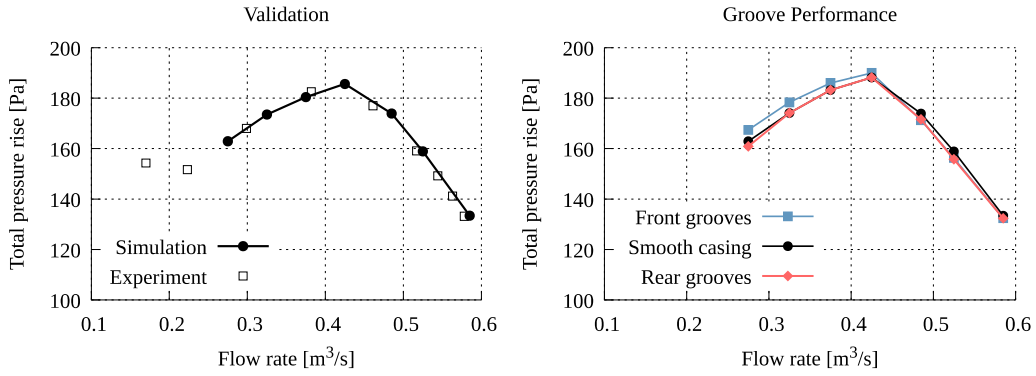

Fig. 1. Total pressure rise as function of flow rate: Comparison between simulation and experiment (left), influence of grooves on top of the front or rear rotor compared to a smooth casing (right).

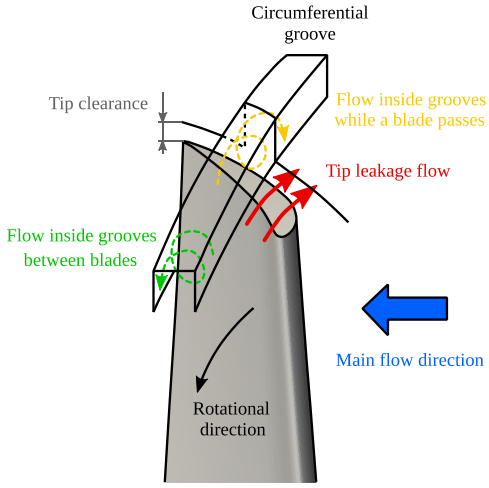

Fig. 2. Sketch of the flow structure inside the grooves.

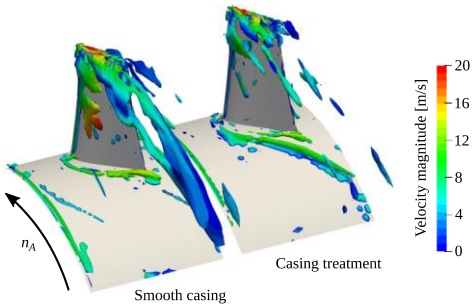

Fig. 3. Time-averaged λ_2 iso-surfaces showing the tip leakage vortex for smooth casing (left) and casing treatment (right) for the front rotor at Q = 0.325 m^3/s.

the groove at the pressure side of the blade and leaves at the suction side. As a result, the flow direction inside the grooves reverses and moves in the opposite circumferential direction as the blade.

Figure 7 visualizes the positive effect of circumferential grooves on the tip-leakage flow at Q = 0.325 m^3/s. The time-averaged λ_2 criterion is used to identify vortices in the three-dimensional velocity field downstream of the blades at the front rotor. Compared to the smooth casing setup, the tip-leakage vortex with casing treatment has a significantly reduced intensity. It breaks down more quickly and gets pushed slightly in an axial direction. As a result, lower velocity gradients lead to reduced shear stresses and thus losses in the flow field. Furthermore, the flow is less disturbed and fluctuations are reduced. This effect is especially important for contra-rotating fans, where the tip leakage vortex of the front rotor eventually hits the rear rotor.

Weakened tip-leakage flow results in lower pressure fluctuations on the blade surfaces. Figure 8 shows the static pressure standard deviation on the suction surface for the front and rear rotor in case of a smooth casing, front grooves, and rear grooves at Q = 0.325 m^3/s. The overall level of fluctuations is similar for all three configurations. However, grooves reduce the static pressure standard deviations at the leading edge and the tip region of the blades. This can be seen by comparing the front rotor with and without grooves. Lower oscillations result from the improved flow field in the tip clearance region due to weakened tip leakage vortex.

The rear rotor also benefits from grooves on top of the front rotor. The weakened tip leakage vortex downstream of the front rotor results in a less disturbed inflow for the rear rotor. This reduces the pressure fluctuations near the tip region and at the leading edge between the tip and midspan. As a result, blade-to-blade interactions between the front and rear rotors are reduced. This also explains why grooves on top of the rear rotor have less effect on fan performance. Although they likewise reduce pressure fluctuations near the tip of the blade, there is no downstream rotor to benefit from reduced disturbances in the flow field. The strong oscillations at 50 % span at the rear rotor result from flow separation occurring at the front rotor. The resulting vortices hit the rear blade and result in large pressure fluctuations. Grooves cannot mitigate this effect.

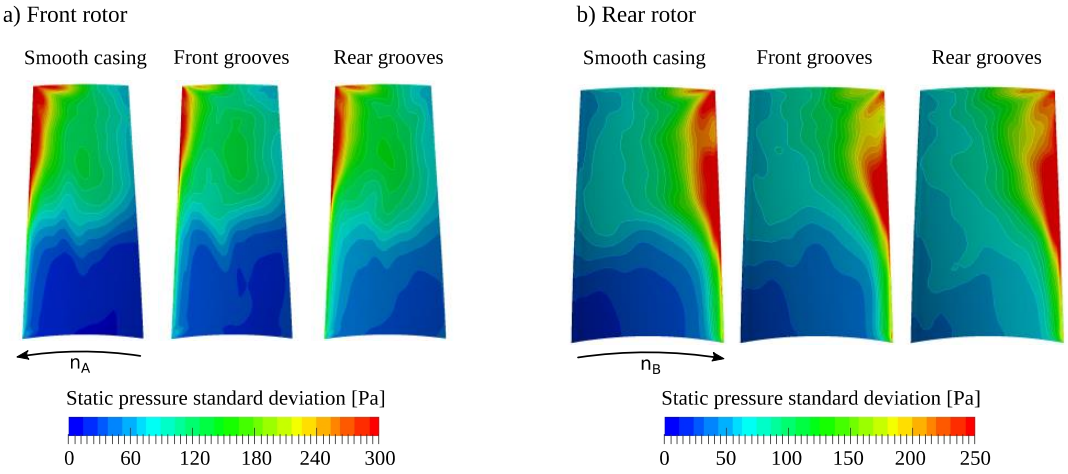

Fig. 8. Static pressure fluctuations on the suction surface of a) front and b) rear rotor for a smooth casing, front, and rear grooves at Q = 0.325 m³/s.

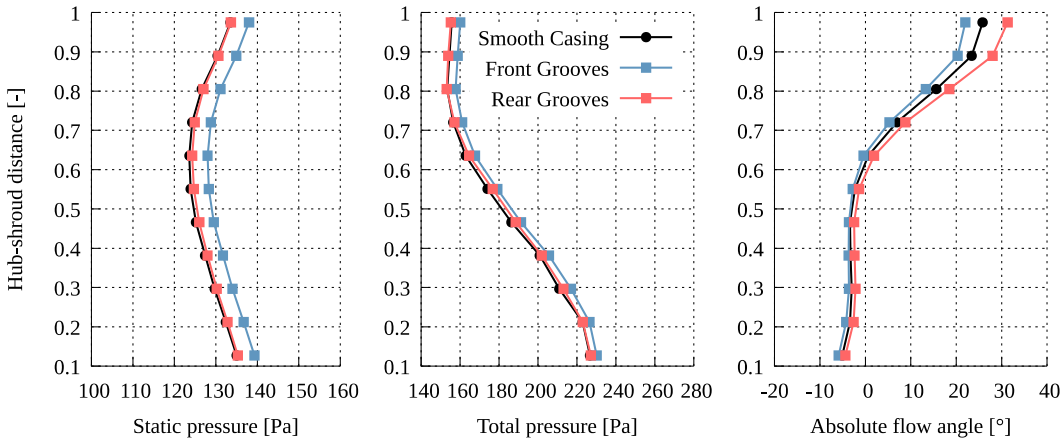

Fig. 9. Static pressure (left), total pressure (center), and absolute flow angle (right) downstream the rear rotor between hub and shroud for smooth casing, front, and rear grooves at Q = 0.325 m³/s.

4.3 Numerical Pressure Probes

Several probes are used to investigate fluctuations in the flow field downstream of the fan stage. They are placed 20 mm downstream of the rear rotor and arranged in radial direction from hub to shroud. They monitor static and total pressure and the absolute flow angle. Figure 9 shows the time-averaged values for all three variables at a flow rate of Q = 0.325 m³/s. The static pressure is distributed quite evenly between hub and shroud (Fig. 9, left). Similar to the findings regarding the fan performance, front grooves result in the highest static pressure while rear grooves and smooth casing are nearly identical. Total pressure variations show significantly higher values close to the hub (Fig. 9, center). Again, a contra-rotating fan with grooves on top of the front rotor yields the best performance. This is in line with the higher total pressure rise of the contra-rotating fan with grooves on top of the first rotor.

The absolute flow angle is shown in Fig. 9 (right). Its value is close to zero in the lower half of the flow channel indicating a nearly perfectly axial flow field downstream of the fan stage. This is due to the rear rotor, which recovers part of the kinetic energy of the swirl coming from the front rotor. However, close to the shroud, this value rises up to 30°. This follows from flow separation at midspan at the front rotor and the tip leakage vortex. Grooves on top of the front rotor reduce this value by up to 4° close to the shroud. This results from the weakened tip leakage vortex, which is pushed more towards an axial direction. In contrast, grooves on top of the rear rotor increase the absolute flow angle and thus strengthen the swirl in the flow. As a result, more energy is not recovered.

Analyzing the characteristic frequencies of the flow downstream the rear rotor gives further insight into the influence of grooves onto the flow field. For this reason, a fast Fourier transform is performed on 5 of the pressure probes as shown in Fig. 10. Their positions range from 22 % to 94 % span at a distance of 20 mm downstream of the rear rotor. They are fixed in space, e.g. not moving with the blades.

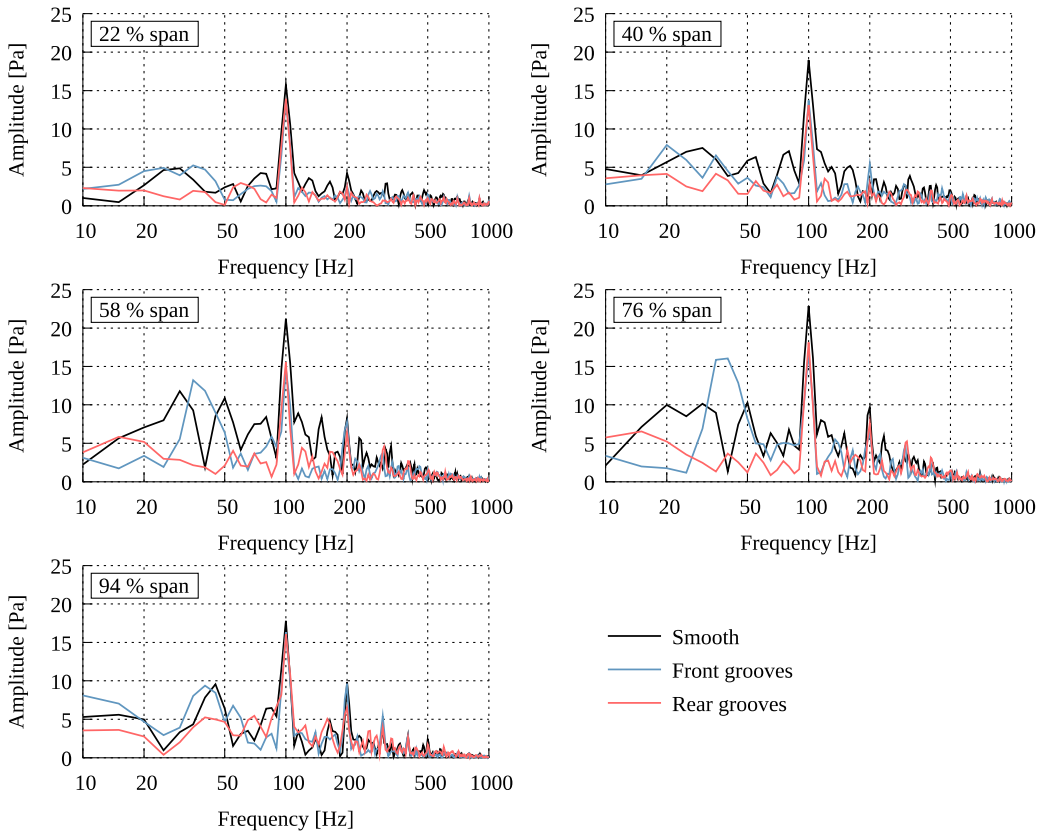

Fig. 10. FFT of pressure fluctuations downstream of the fan stage at different span for smooth casing, front grooves, and rear grooves rotor at Q = 0.325 m^3/s.

The main characteristics are the blade passing frequency (BPF) of the front and rear rotor at 224 Hz and 100 Hz, respectively, and their harmonics. Casing treatment on either the front or rear rotor changes the magnitude of these frequencies. At midspan and close to the hub, grooves significantly decrease the intensity of the BPF. Furthermore, the overall intensity is reduced for frequencies above 100 Hz. At the same time, lower frequencies are partly increased, though. For example, there is a new peak around 40 Hz at 58 % and 76 % span. The reason for the reduced BPF intensity can be found in the weakened tip leakage vortices as shown in the λ_2 iso-surfaces. This results in lower pressure fluctuations downstream of the fan stage.

5. CONCLUSIONS

The benefits of circumferential groove casing treatment on a low-speed contra-rotating fan have been investigated numerically. Grooves were either placed on top of the front or rear rotor and compared with a smooth casing without treatment. The transient simulations were performed and time-averaged over several rotations. After analyzing the results, the following conclusions can be made:

- Grooves on top of the front rotor increase the fan performance by up to 4 % compared to a smooth casing. This effect is achieved in particular at off-design conditions and low flow rates. For other operating conditions, smooth casing yields the best results. Rear grooves do not offer any significant advantage.
- The positive effect of grooves can be attributed to the significantly weaker tip leakage vortex as shown in the λ_2 iso-surfaces. Lower velocity gradients lead to reduced shear stresses and therefore pressure losses.
- As an effect, pressure fluctuations at the leading edge and close to the tip region of the blades are reduced. This is also the case for the rear blade if grooves are placed on top of the front rotor. A weaker tip leakage vortex leads to a less disturbed inflow for the rear rotor and thus fluctuations.
- Grooves on top of the rear rotor offer no positive effect since there is no third rotor downstream to benefit from reduced fluctuations or reduced tip leakage vortex.
- The positive influence of grooves can also be shown downstream of the contra-rotating fan. By using an FFT, characteristic frequencies were identified for several pressure probes. As a result, grooves tend to reduce the magnitude of blade passing

frequencies and their harmonics while partly increasing lower frequencies.

Further investigations should focus on the influence of groove properties, such as groove placement, size, orientation, and shape. Furthermore, acoustic simulations or experiments can be performed to analyze the effect of grooves on the sound emissions of contra-rotating fans. The latter is particular of interest due to the generally higher acoustic emissions of contra-rotating fans compared to single-rotor fans.

REFERENCES

ANSYS TurboGrid (2018), www.ansys.com.

Bailey, E. E. (1972). Effect of grooved casing treatment on the flow range capability of a single-stage axial-flow compressor. *Technical Report NASA TM X-2459*.

Caretto, L. S., A. D. Gosman, S. V. Patankar and D. B. Spalding (1972). Two Calculation Procedures for Steady, Three-Dimensional Flows with Recirculation. *Proceedings of the Third International Conference on Numerical Methods in Fluid Mechanics*, Paris, France.

CFturbo (2017), version 10.3.

Chen, Y., B. Lui, Y. Xuan and X. R. Xiang (2008). A study of speed ratio affecting the performance of a contra-rotating axial compressor. *Proc IMechE, Part G: Journal of Aerospace Engineering* 222(7), 985-991.

Egorov, Y. and F. R. Menter (2008). Development and Application of SST-SAS Model in the DESIDER Project. *Symposium of Hybrid RANS-LES Methods*, Corfu, Greece.

Issa, R. I. (1986). Solution of the implicitly discretized fluid flow equations by operator-splitting. *Journal of Computational Physics* 62(1), 40-65.

Kerscher, M., G. Heilmann, C. Puhle, R. Krause and C. Friebe (2017). Sound Source Localization on a Fast Rotating Fan Using Rotational Beamforming. *INTER-NOISE*, Hong Kong, China.

Krause, R., C. Friebe, M. Kerscher and C. Puhle (2018). Investigations on noise sources on a contra-rotating axial fan with different modifications. *FAN 2018*, Darmstadt, Germany.

Mao, X., B. Liu and H. Zhao (2018). Numerical analysis of the circumferential grooves casing treatment in a counter-rotating axial flow compressor. *Applied Thermal Engineering* 130, 29-39.

Menter, F. R. (1994). Two-equation eddy-viscosity turbulence models for engineering applications. *AIAA Journal* 32(8), 31-35.

Mistry, C. and A. Pradeep (2012). Effect of variation in axial spacing and rotor speed combinations on the performance of a high aspect ratio contra-rotating axial fan stage. *Proc IMechE, Part A: Journal of Power and Energy* 227(2), 138-146.

Muller, M. W., H. P. Schiffer and C. Hah (2007). Effect of circumferential grooves on the aerodynamic performance of an axial single-stage transonic compressor. *ASME Turbo Expo 2007: Power for Land, Sea, and Air*, Montreal, Canada.

Nagano, S., H. Takata and Y. Macmida (1971). Dynamic Performance of Stalled Blade Flow. *Bulletin of JSME*, 11.

Nouri, H., F. Ravelet, F. Bakir, C. Sarrafa and R. Rey (2012). Design and Experimental Validation of a Ducted Counter-rotating Axial-flow Fans System. *Journal of Fluids Engineering* 134(10), 1-6.

OpenFOAM (2018), version v1812.

Pundhir, D. S., P. B. Sharma and K. K. Chaudhary (1990). Effect of casing treatment on aerodynamic performance of a contrarotating axial compressor stage. *Proc IMechE, Part A: Journal of Power and Energy* 204(1), 47-55.

Rabe, D. C. and C. Hah (2002). Application of casing circumferential grooves for improved stall margin in a transonic axial compressor. *ASME Turbo Expo 2002: Power for Land, Sea, and Air*, Amsterdam, The Netherlands.

Roy, B., P. Rao, S. Basu, A. Raju and P.N. Murthy (1992). Flow studies in ducted twin-rotor contra-rotating axial flow fans. *International Gas Turbine and Aero Engine Congress and Exposition*, Cologne, Germany.

Sharma, P., Y. Jain and D. Pundhir (1988). A study of some factors affecting the performance of a contra-rotating axial compressor stage. *Proc IMechE, Part A: Journal of Power and Energy* 202(1), 15-21.

Sharma, P. B., Y. P. Jain, N. K. Jha and B. B. Khanna (1985). Stalling Behavior of a Contra-Rotating Stage. *7th International Symposium on Air Breathing Engines*, Peking, China.

Wang, J., F. Ravelet and F. Bakir (2013). Experimental comparison between a counter-rotating axial flow fan and a conventional rotor-stator stage. *10th European Turbomachinery Conference*, Lappeenranta, Finland.

Wang, Y., W. Chen, C. Wu and S. Ren (2014). Effects of tip clearance size on the performance and tip leakage vortex in dual-rows counter-rotating compressor. *Proc IMechE, Part G: Journal of Aerospace Engineering* 229(11), 1953-1962.

Wu, Y. H., W. L. Chu, H. Zhang and Q. Li (2010). Parametric investigation of circumferential grooves on compressor rotor performance. *ASME Journal of Fluids Engineering* 132(12), 1-10.